Annals of Biomedical Engineering manuscript No.
(will be inserted by the editor)

Automatized Patient-Specific Methodology for Numerical Determination of Biomechanical Corneal Response

M. A. Ariza-Gracia, J. Zurita, D. P. Piñero, B. Calvo,

J. F. Rodríguez

the date of receipt and acceptance should be inserted later

Abstract The availability of high resolution topographical data and the patient's IOP have make possible to reconstruct a patient's specific geometric model of the cornea, which makes possible to study specific treatments and pathologies. This work presents a novel methodology for building a three dimensional patient-specific eyeball model suitable for performing a fully automatic finite element analysis of corneal biomechanics. The proposed pipeline incorporates an algorithm to determine the initial stress in the cornea due to the IOP. An automatic reconstruction algorithm fits the patient's corneal surfaces, obtained by means of a topographer, and creates a FE mesh for the simulation. The fitting process, however, respects the patient's corneal elevation and pachymetry data obtained from the topographer in order to account for all corneal geometric features in the analysis. The methodology is demonstrated with the simulation of a non-contact tonometry diagnostic test on 127 patients: 52 healthy eyes, 60 keratokonic eyes, and 15 post-LASIK surgery eyes. Results obtained from the simulations are in good agreement with clinical results reported in the literature, and demonstrate the importance of considering the initial corneal presstres induced by the IOP in the finite element analysis. The potential and flexibility of the proposed methodology allows to improve the understanding of the eye biomechanics, as well as helping to plan surgeries, i.e., LASIK surgeries, or to interpret the results of new diagnosis tools, as in the case of non-contact tonometers.

Keywords corneal model, patient specific, non-contact tonometry

M. A. Ariza-Gracia B. Calvo, J. F. Rodríguez
Applied Mechanics and Bioengineering (AMB). Aragón Institute of Engineering Research (I3A). University of Zaragoza, Zaragoza, Spain.
E-mail: mariza@unizar.es

B. Calvo
Bioengineering, Biomaterials and Nanomedicine Online Biomedical Research Center (CIBBER-BBN)

D. P. Piñero
Ophthalmology Department (OFTALMAR), Medimar International Hospital, Alicante (Spain).
Optics, Pharmacologist and Anatomy Department, University of Alicante (Spain).

J. Zurita
Department of Mechanical Engineering, Energetics and Materials, Public University of Navarra (Spain).

1 Introduction

The corneal shape is the result of the equilibrium between its mechanical stiffness (related to corneal's geometry and the intrinsic stiffness of the corneal tissue), intraocular pressure (IOP) and the external forces acting upon it such as an external pressure. An imbalance between these parameters, e.g. an increment of IOP (glaucoma), a decrement of the corneal thickness induced by a refractive surgery or a corneal material weakening due to a disruption of collagen fibres (keratoconus), can produce ocular pathologies (ectasias) which seriously affect patient's sight. Consequently, it is important to understand how ocular factors such as IOP, geometry and corneal material are related to pathologies in order to improve treatments. The first step in this direction consists in the correct measurement of the IOP and corneal topography. To date, the IOP is measured by either contact tonometers (e.g. Goldmann Applanation Tonometry) [24,17] or non–contact tonometers (e.g. CorVis ST)[11], whereas, the corneal topography is obtained with corneal topographers (e.g. Pentacam and Sirius)[3], which have reached a high level of sophistication and accuracy.

The availability of high resolution topographical data and the patient's IOP have make possible to reconstruct a patient's specific geometric model of the cornea, which makes possible to study specific treatments and pathologies. In this regard, some patient-specific corneal models have been reported in the literature[23,25]. However, the pipeline described in these studies cannot be automated in a straightforward manner as to permit personalised analysis on large populations. Another limitation is that these methodologies rely on an approximation of the topographical data when building the corneal model. Studer et al.[25] used Zernike polynomials to generate anterior and posterior corneal surfaces by approximating the available topographical data instead of directly incorporating the corneal thickness and curvature provide by the topographer. In addition, these numerical models did not provide appropriate mesh sensitivity analysis in order to check the accuracy of the results.

An accurate numerical model of the eye relies on the identification of an adequate strain energy function from which the stress-strain relationship of the cornea is obtained. In order to do this, it is first necessary to understand the underlying structure of the tissue. In this regard, the cornea is composed of four different layers: epithelium, bowman's membrane, stroma and endothelium. The stroma represents the major part of the cornea and is formed by different orthogonally crossed lamellae, which are made of collagen fibres. The corneal collagen is organized in two preferential directions:[15,16] i) Nasal–Temporal direction, and ii) Superior–Inferior direction. On the contrary, limbus collagen fibres are disposed circumferentially[20,18,19]. These characteristics provide the cornea with a highly anisotropic behaviour in addition to a nearly incompressible response.[4] Even though the cornea shows an intrinsic viscoelastic behaviour, for most applications it maybe described as a nonlinear anisotropic hyperelastic solid[18,19,15]. In addition to these considerations on the mechanical response, it must be noticed that

topographers measure the geometry of the cornea under the action of the IOP. Therefore, it is necessary to obtain a free-stress configuration of the eyeball that faithfully represents the load free configuration of the cornea. Elsheikh et al.[7] and Roy et al.[23] proposed an iterative geometrical algorithm by varying IOP in order to obtain the reference eyeball geometry, whereas Studer et al.[25] and Lanchares et al.[15] proposed a pre-stressing algorithm based on the deformation gradient. However, these algorithms did not incorporate a consistent mapping of the direction of collagen fibbers into the identified load free configuration. Riveros et al.[21] have proposed a general pullback algorithm for nonlinear anisotropic materials in which the direction of collagen fibres is consistently mapped into the identified zero pressure configuration.

The aim of this work is to develop a robust methodology to incorporate a patient's specific corneal topology into a finite element (FE) model of the eyeball. The proposed methodology accounts for the stress-free configuration of the eyeball and takes into account the hyperelastic anisotropic material response of the corneal tissue. The proposed pipeline is demonstrated on a set of 127 patients (52 healthy eyes, 60 keratoconic eyes and 15 eyes subjected to a LASIK surgical procedure) following a non-contact tonometry protocol. Results are compared with data reported in the literature from simulation[14,28] and clinical studies.[22,9]

2 Methods

Figure 10 shows the proposed pipeline for the patient specific corneal modelling. The framework comprises five main steps namely: i) topographic characterisation of the patient's cornea, ii) corneal geometric reconstruction , iii) eye ball finite element model generation, iv) imposition of the initial stress due to the IOP, and v) computer simulation of the eye ball. Each of these steps is described in the following.

2.1 Topographic data acquisition

Corneal data is obtained with a Pentacam topographer as point cloud surfaces in the form of two 141x141 matrices. The first matrix gives the coordinates (x, y, z) of the anterior corneal surface, whereas the second matrix represents the available pachymetry data at each (x, y) point. Since pachymetry data is sometimes not available at all points in the anterior surface point cloud, the number of non-zero elements in the pachymetry matrix determines the total number of available data points for surface reconstruction. The posterior surface is obtained from the anterior surface and the pachymetry data by point-to-point substraction.

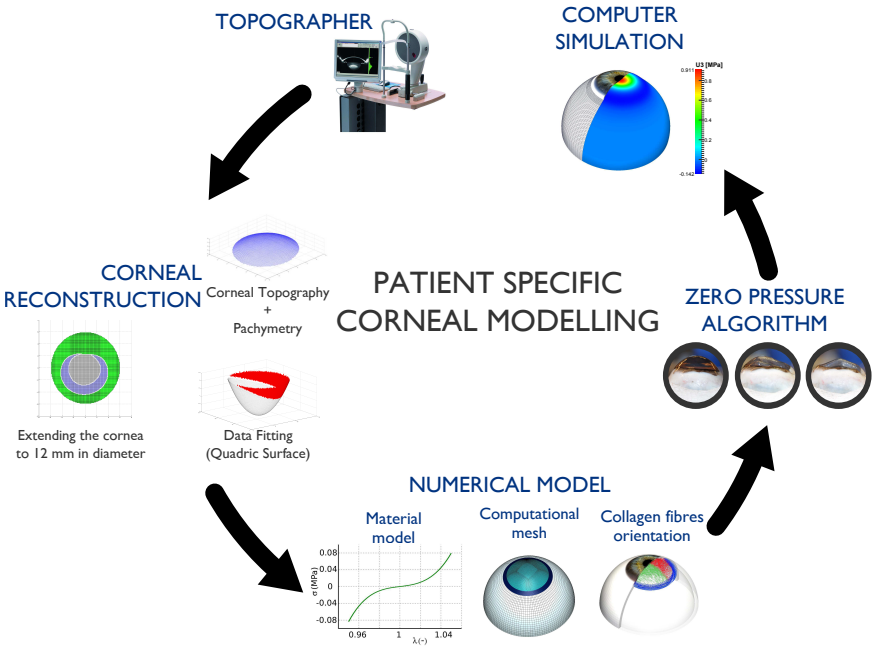

Fig. 1 General pipeline of the propose framework for patient specific corneal modelling.

2.2 Corneal surface reconstruction

A reliable patient specific FE model of the cornea must incorporate patient's topographical data as much as possible. In this regard, the propose framework makes use of actual patient's data where available, while minimising the amount of extrapolated data required to build a full three-dimensional FE model amenable for numerical simulations. Current topographers provide topographical data limited to a corneal area between 8 to 9 mm in diameter (see Fig. 11A). However, for building a 3D model, a corneal diameter of 12 mm (average human size) is needed.[23,25]

In order to overcome this limitation, a surface continuation algorithm is proposed. Data extrapolation is performed by means of a quadric surface given in matrix notation as

$$\mathbf{x}^T\mathbf{A}\mathbf{x} + 2\mathbf{B}^T\mathbf{x} + c = 0, \tag{1}$$

where $\mathbf{A}$ is a 3×3 constant matrix, $\mathbf{B}$ is a 3×1 constant vector, and c is an scalar which define the parameters of the surface. Equation 1 is fitted to the topographical data by means of a nonlinear regression analysis.

For extending the corneal surface, it is desirable that Eq. 1 approximates well the periphery of the patient's topographical data (blue area in Fig. 11A). For this reason, previously to fitting Eq.1, the central part of the corneal is removed using a level set algorithm based on the relative elevation of each corneal point with respect to the apex. In brief, starting at a relative elevation of 1, i.e., the apex, and reducing in steps of 0.005, subsequent level sets are identified (see grey area in Fig. 11A). When the size of the level set, i.e., radius of the circumscribe circle, changes less than a 15% between two consecutive

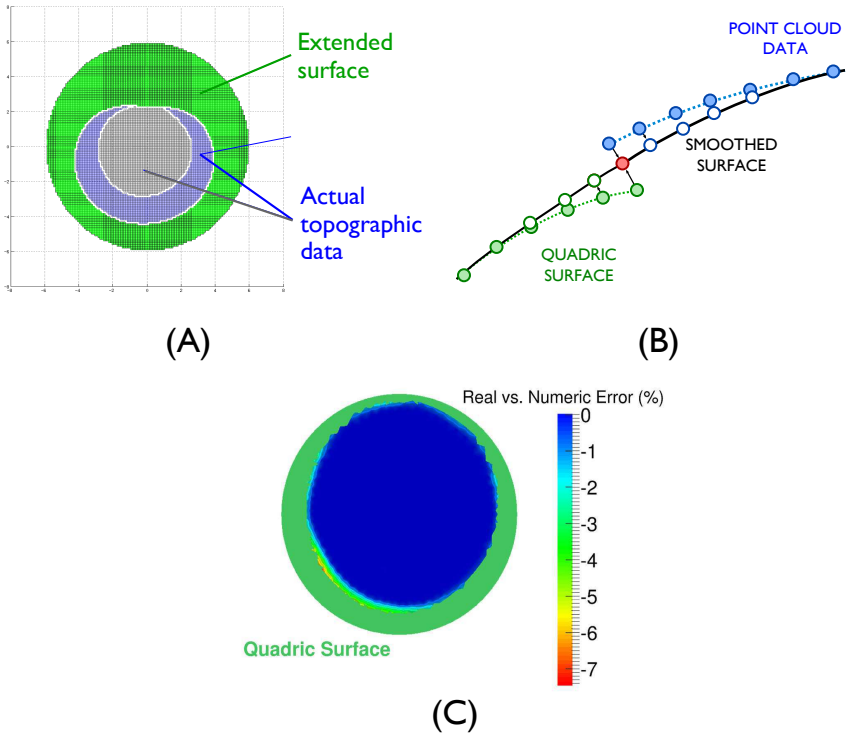

Fig. 2 Corneal surface reconstruction. A) Projection of the 12 mm diameter corneal surface in the optical axis plane. Grey and blue shaded surfaces correspond to the corneal surface measured by the topographer. Green area corresponds to the extended surface required in order to achieve a 12 mm diameter. B) Surface smoothing at the joint between the extended surface and the patient's corneal surface. C) Contour map of the error between the point cloud data prior and after smoothing

increments, the algorithm stops. Corneal periphery is then obtained by subtracting the identified level set from the topographic data (blue area in Fig. 11A).

When using an analytical surface as Eq. 1 to extend the corneal surface, there will always be a jump at the joint between the approximating surface and the point cloud surface (see Fig. 11B). This discontinuity in the surface normal may lead to convergence problems or to non realistic stress distributions of the cornea during the FE analysis. Therefore, a smoothing algorithm based on the continuity of the normal between the quadric surface and the point cloud surface is applied as shown in Fig. 11B. This procedure will produce small alterations in the patient's topographic data near the border. However, this alterations are very small as demonstrated in Fig. 11C by the contour map of the error between the point cloud data prior and after smoothing (data corresponds to a typical patient).

2.3 Numerical model of the cornea

2.3.1 Material Description

The cornea is considered as an anisotropic hyper elastic material. The Gasser–Holzapfel–Ogden's strain energy function (G–H–O)[8,10] is proposed for describing the constitutive behaviour of the cornea.

$$U = \frac{1}{D}\cdot\left(\frac{J_{el}^2-1}{2} - ln(J_{el})\right) + C_{10}\cdot(\bar{I}_1-3) + \frac{k_1}{2\cdot k_2}\cdot\sum_{\alpha=1}^{N}\{\exp[k_2\langle\bar{E}_\alpha\rangle^2]-1\}$$
$$\bar{E}_\alpha \overset{\text{def}}{=} \kappa\cdot(\bar{I}_1-3) + (1-3\kappa)\cdot(\bar{I}_{4(\alpha\alpha)}-1), \tag{2}$$

where $\bar{I}_1$ is the first invariant of the modified right Cauchy-Green tensor $\bar{C} = J_{el}^{-2/3}C$, J_{el} is the elastic volume ratio, $\bar{I}_{4(\alpha\alpha)}$ is a pseudo-invariant that represents the square of the stretch along the direction of the α^{th} family of collagen fibres, being N the total number of families of collagen fibres (see Fig.12.D). D represents the inverse of the volumetric modulus. The dispersion parameter, κ, $(0 \leq \kappa \leq \frac{1}{3})$ determines the anisotropic grade: $\kappa = 0$ implies transversely isotropy, and $\kappa = 3$ implies isotropy. In addition, Eq. 2 assumes that collagen fibres only work under traction, i.e. $\bar{E}_\alpha > 0$.

The material constants for the corneal and limbal constitutive model were obtained by means of non-linear regression analysis of a typical IOP-apical rise curve:[28] $C_{10} = 0.05$ [MPa], $D = 0.0$ [MPa^{-1}], $k_1 = 130.9$ [MPa], $k_2 = 2490.0$ [–] and $\kappa = 0.33329$ [–]. For the computations, the same mechanical properties and dispersion parameter have been assumed for all families of fibres. Figure 12A-B show the stress-stretch and IOP-apical rise curves predicted with the proposed material model. Fig. 12B demonstrate that the IOP-apical rise curve is within the reported human range[28].

The sclera has been assumed as an isotropic hyperelastic material[6]

$$U = \sum_{i=1}^{3}\frac{1}{D_i}(J_{el}-1)^{2\cdot i} + \sum_{i=1}^{3}C_{i0}\cdot(\bar{I}_1-3)^i, \tag{3}$$

with $C_{10} = 0.81$ [MPa], $C_{20} = 56.05$ [MPa], $C_{30} = 2332.26$ [MPa], $D = 0.0$ [MPa^{-1}].

2.3.2 Finite Element model

Once the surface fitting has been completed, it is inserted in a three-dimensional geometric model of the anterior half ocular globe geometry, which accounts for three different parts: the cornea, the limbus and the sclera. The sclera was assumed as a 28 mm diameter sphere and constant thickness of 1 mm, whereas the limbus is a ring linking both, sclera and cornea. The geometry has been meshed using hexahedral elements by means of an in-house C program as shown in Fig. 12C. The software allows for a precise control of the mesh size, as well as generating meshes with trilinear (8-nodes) or quadratic (20-nodes) hexahedral elements. Pachymetry data measured with the topographer is accurately mapped into the three dimensional finite element model during mesh generation. The finite element model of the eye ball is completed by the definition of two fibre directions in the cornea (a nasal-temporal and superior-inferior directions) and one circumferential direction in the limbus as shown in Fig. 12D.

Symmetry displacement boundary conditions have been defined in the base of the sclera (Π plane in Fig. 12C)[20,15] in such a way that cornea will not be perturbed by boundary hypothesis, and the eyeball

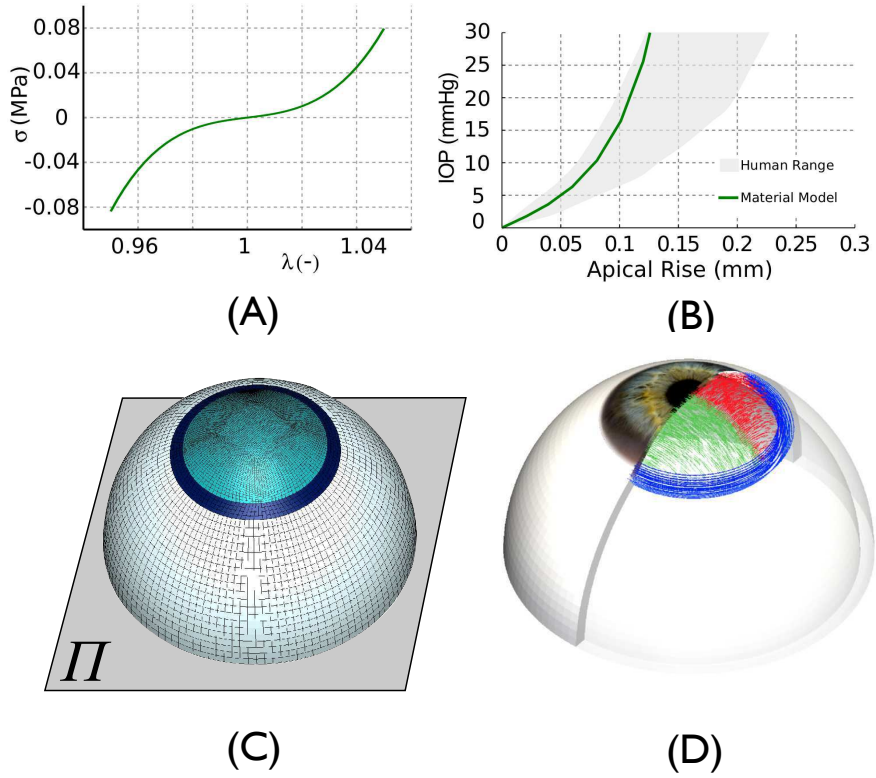

Fig. 3 Numerical model of the eye ball. A) Stress-stretch curve for the corneal material model. B) IOP-apical rise curve predicted by the material model. The grey area corresponds to the reported human range[28]. C) Finite element mesh of the eye ball: Sclera (white region), Limbus (dark blue region), cornea (light blue region). D) Direction of collagen fibres. Two orthogonal directions for the cornea (red and green fibres), and one circumferential direction (blue fibres) for the limbus.

is allowed to move along the radial direction on the symmetry plane. This boundary condition is much less restrictive than fixing all degrees of freedom of nodes at the symmetry plane.[23, 25] The inner surface of the eyeball is subject to the patient's IOP.

Computation time and accuracy are both the most important parameters when conducting a FE analysis. Unfortunately, the higher the accuracy the higher the computation time required. In order to reach an optimal compromise between accuracy and computation time a sensitivity analysis of the finite element model was performed. Linear and quadratic elements where considered, and the number of elements through the corneal thickness was varied from 2 to 8 elements (4, 6, and 8 for linear elements, and 2, 3, 4, and 5 for quadratic elements). In addition, the maximum element size was varied from 0.3 mm to 0.2 mm. Maximum apical displacement, and maximum principal stress have been considered as monitor variables in the convergence analysis. The sensitivity analysis was performed based on the simulation of a non contact tonometry test. In this regard, the air-puff acting on the anterior corneal surface was assumed as a metered collimated air pulse with a peak pressure of 25 kPa (180 mmHg) and 30 ms duration, as shown in Fig. 13A. The spatial distribution of the pressure due to the air-puff (see Fig. 13B) was defined from a CFD simulation performed with the commercial software ANSYS (ANSYS, Inc.) in order to obtain a realistic pressure distribution.[1] The FE analysis was performed using the commercial finite element software ABAQUS (Dassault Systemes Simulia Corp.). The anisotropic material model for

the cornea and limbus were implemented in the material user subroutines UANISOHYPER_INV within ABAQUS.

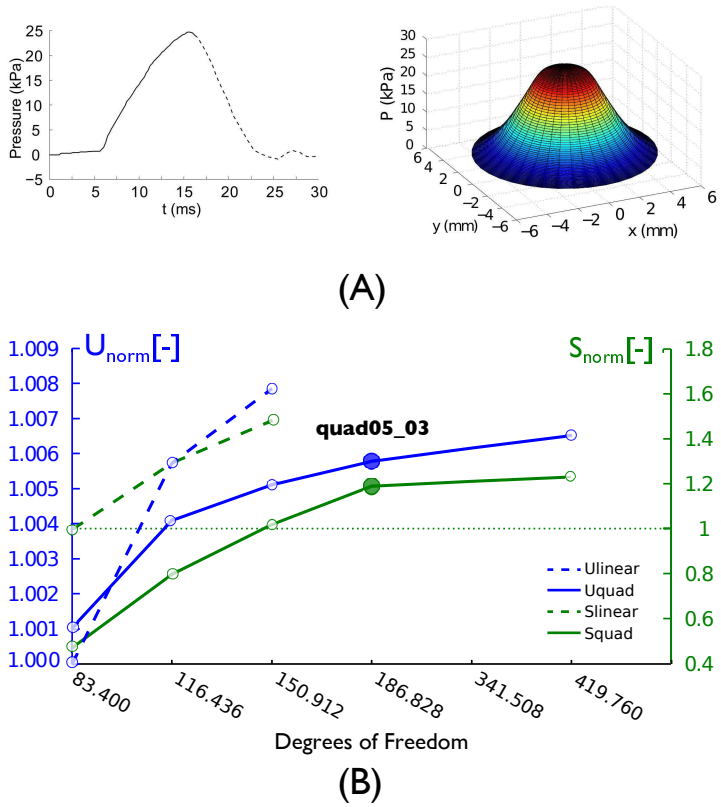

Fig. 4 Mesh sensititvity analysis of the FE model. A) Temporal pressure profile applied on the center of the cornea to simulate a non-contact tonometry test. Solid black line represents the temporal profile used in the simulations. B) Spatial pressure profile applied on the cornea's anterior surface obtained by means of a CFD simulation.

Figure 13B shows the maximum apical displacement and maximum principal stress in the cornea as a function of the mesh size. Results in Fig. 13B have been normalised with respect to those obtained for the coarsest mesh. In general, trilinear elements show a much slower rate of convergence as compared to quadratic elements, in addition to predict a slightly larger apical displacement and larger stresses. In this regard, Fig. 13 shows that when using quadric elements, for a mesh with more than 186000 degrees of freedom (62000 nodes) the maximum apical displacement and maximum principal stress change less than 0.05% and 5% respectively. Another remarkable aspect of the sensitivity analysis concerns the computation time. A model with 186000 degrees of freedom made with trilinear hexahedra takes about three times more computing time as the equivalent model meshed with quadratic elements (results not shown).

Based on the sensitivity analysis, the FE model is generated with quadratic hexahedra and five elements through the thickness (11 nodes through the thickness). The resulting eyeball has 62276 nodes (186828 degrees of freedom) and 13425 quadratic elements.

2.4 Zero Pressure Algorithm

When an eye is measured by a topographer, the identified geometry corresponds to a deformed configuration due to the effect of the IOP. Hence, an accurate stress analysis of the cornea starts by identifying the initial state of stresses due to the IOP, or equivalently, the unloaded geometry of the eye (geometry associated with the absence of IOP) as shown in Fig. 14A. Figure 14.B shows the iterative algorithm used to find the unloaded configuration of the eye.[21] The algorithm keeps the mesh connectivity unchanged and iteratively updates the nodal coordinates. The local directions of anisotropy (orientation of collagen fibres) is also consistently pulled-back to the current zero-pressure configuration.

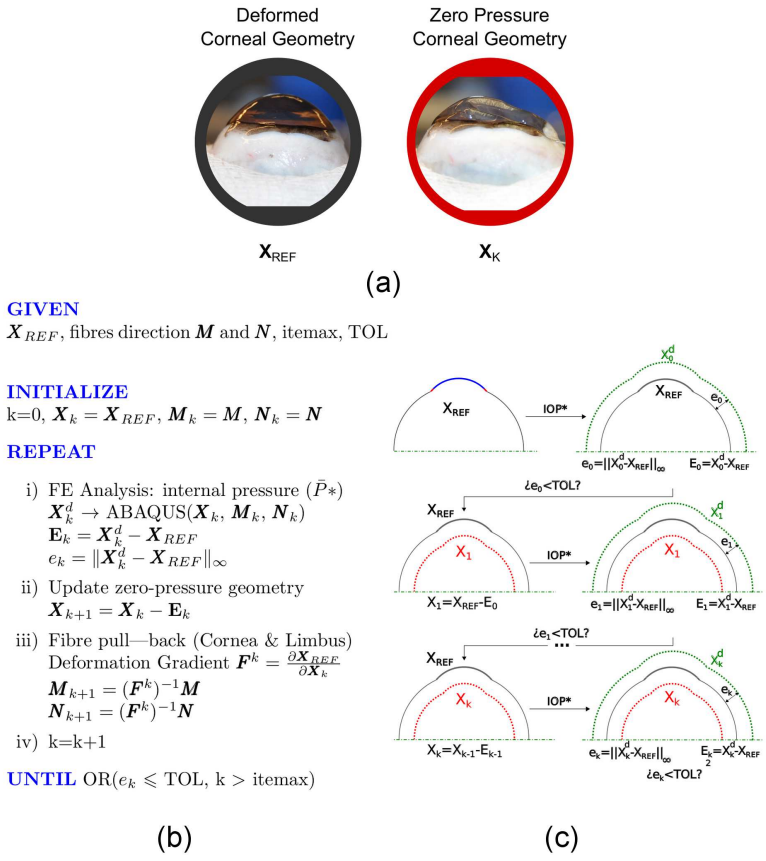

Fig. 5 (A) Influence of the IOP in the corneal shape (dog's cornea); (B) Pull-back algorithm with consistent mapping of the fibres to the current unloaded state; (C) Scheme of the algorithm.

In Fig. 14, $\mathbf{X}_{REF}$ stands for the patient's geometry reconstructed from the topographer's data, where $\boldsymbol{X}$ represents a $N_n \times 3$ matrix that stores the nodal coordinates of the finite element eyeball, with N_n the number of nodes in the FE mesh, i.e., 62276 nodes; $\mathbf{X}_k$ is the zero pressure configuration identified at iteration k; and $\mathbf{X}_k^d$ is the deformed configuration obtained when inflating the zero-pressure configuration $\mathbf{X}_k$ at the IOP pressure. The iterative algorithm updates the zero pressure geometry, $\mathbf{X}_k$, until the infinite norm of the nodal error between $\mathbf{X}_{REF}$ and $\mathbf{X}_k^d$ is less than a tolerance, TOL. The algorithm is described as follows:

Initialization: Fibre directions, $\mathbf{M}$ and $\mathbf{N}$, are defined in the reconstructed corneal geometry. Tolerance TOL and maximum number of iterations $itemax$ are defined, and counter k is initialized.

Step i: At the $k+1$-th iteration a FE stress analysis is performed considering the zero pressure configuration computed in the k-th iteration as the reference configuration to obtaine $\mathbf{X}_k^d$, the deformed configuration at k-th iteration. Boundary conditions and IOP are applied as described in the previous section.

Step ii: The $k+1$-th zero-pressure geometry is computed as $\mathbf{X}_{k+1} := \mathbf{X}_k - (\mathbf{X}_k^d - \boldsymbol{X}_{REF})$.

Step iii: The fibres are consistently mapped onto the k-th zero-pressure geometry as $\mathbf{M}_{k+1} = (\mathbf{F}_{k+1})^{-1}\mathbf{M}$ ($\mathbf{N}_{k+1} = (\mathbf{F}^{k+1})^{-1}\mathbf{N}$) with the deformation gradient $\mathbf{F}^{k+1} = \partial \mathbf{X}_{REF}/\partial \mathbf{X}_{k+1}$.

Step v: The counter k is incremented.

Step iv: The infinite error norm is computed and if it is less than TOL, or the number of iterations is greater than $itemax$, the algorithm stops.

2.5 Statistical analysis

Statistical analyses were performed in Matlab R2012 v.8.0, and data are reported by their mean and standard deviation (mean ± SD), respectively. Statistical significance was tested with the two-sample Kolmogorov-Smirnov test, where a two-sided p-value of less than 0.05 determined significance.

3 Results

3.1 Corneal reconstruction

The performance of the corneal reconstruction algorithm was demonstrated on three extreme cases: i) a healthy cornea, which is the right cornea of a 50-year woman, with an apex pachymetry of 593 microns, a minimum pachymetry of 586 microns, a nasal–temporal radius of 7.63 mm and a superior–inferior radius of 7.79 mm; ii) a cornea affected by a keratoconus (KTC) corresponding to the left cornea of a 60-year man, with an apex pachymetry and a minimum pachymetry of 499 microns, a nasal–temporal radius of 6.87 mm and a superior–inferior radius of 7.69 mm; and iii) a post LASIK refractive surgery, which is the right cornea of a 60-year woman, with an apex pachymetry of 379 microns, a minimum pachymetry of 375 microns (a very extreme case), a nasal–temporal radius of 11.69 mm and a superior–inferior radius of 11.24 mm.

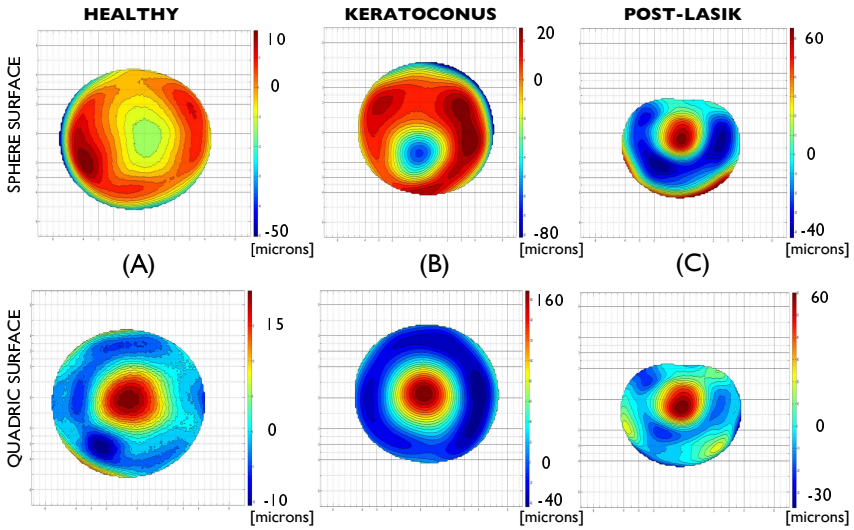

Fig. 6 Subtraction Error, measured on microns (μm), depending on surface fitting typology (Top panel — Sphere / Bottom panel — Quadric): A. Healthy Eye, B. Keratoconus Eye, C. Post-Lasik Eye

The approximation error obtained with the quadric surface and a traditional sphere approximation is shown in Figure 15 for the three eye geometries considered. The figure shows that for the Healthy eye the sphere fits better over corneal apex than corneal borders with an error difference ranging from 33.6 to -74.4 microns (Figure 15.A top panel) whereas the quadric surface fits better over corneal periphery than corneal apex with an error difference ranging from 21.5 to -30.3 microns (Figure 15.A bottom panel). Considering the KTC eye the sphere fits better over corneal center (excepts at the KTC location) than corneal borders with an error difference ranging from 49.9 to -102.2 microns (Figure 15.B top panel), whereas the quadric fits better over corneal periphery than corneal center, where the pathology is very underestimated, with an error difference ranging 180.1 to -57.1 microns (Figure 15.B bottom panel). Regarding the LASIK eye the sphere fits better over corneal center (excepts at the location of the surgery) than corneal borders with an error difference ranging from 71 to -47.4 microns (Figure 15.C top panel) whereas the quadric fits better over corneal periphery than the center of the cornea with an error difference ranging 65.2 to -36.7 microns (Figure 15.C bottom panel). These results indicate that a sphere surface fits better at the center of the cornea while a quadric surface fits better at the periphery of the cornea. Therefore, the *quadric surface model* is better suited to perform the extension of the cornea to reach a 12 mm corneal diameter as required for the FE model.

3.2 Effect of the Zero-Pressure configuration

In order to check the influence of the initial corneal stress due to the zero pressure algorithm in the numerical simulations of eye mechanics, a non-contact tonometry test has been simulated as described in the Methods section. The maximum and the time evolution of the apical displacement has been computed

for three different levels of IOP, i.e., 10 mmHg, 19 mmHg, and 28 mmHg, for the three cases described in the previous section.

Figure 16 shows the apical displacement of the healthy eye for three different IOP, obtained with the zero pressure model (accounting for the initial stress due to the IOP), and with the finite element model build from the topographical images without incorporating the initial stress of the cornea (image based model). The figure shows that incorporating the initial stress of the cornea results on a stiffer corneal response to the air-puff (lower apical displacement), as evidenced in Fig. 16B which shows that the initial stress shifts the maximum apical displacement versus pressure curve. In addition, Fig. 16A shows that the effect of the initial stress is more noticeable as the pressure of the air-puff increases (see Fig. 13A) as demonstrated by the divergence in the apical displacement time course when the initial corneal stress is accounted for. In addition, the divergence between the two curves occurs when the deformation of the cornea becomes significant. Note also that the divergence between the two curves initiates earlier (at a lower air-puff pressure) for lower IOP values as shown in Fig 16A. The behaviour shown in Fig. 16 is also observed in the KTC and post-LASIK geometries.

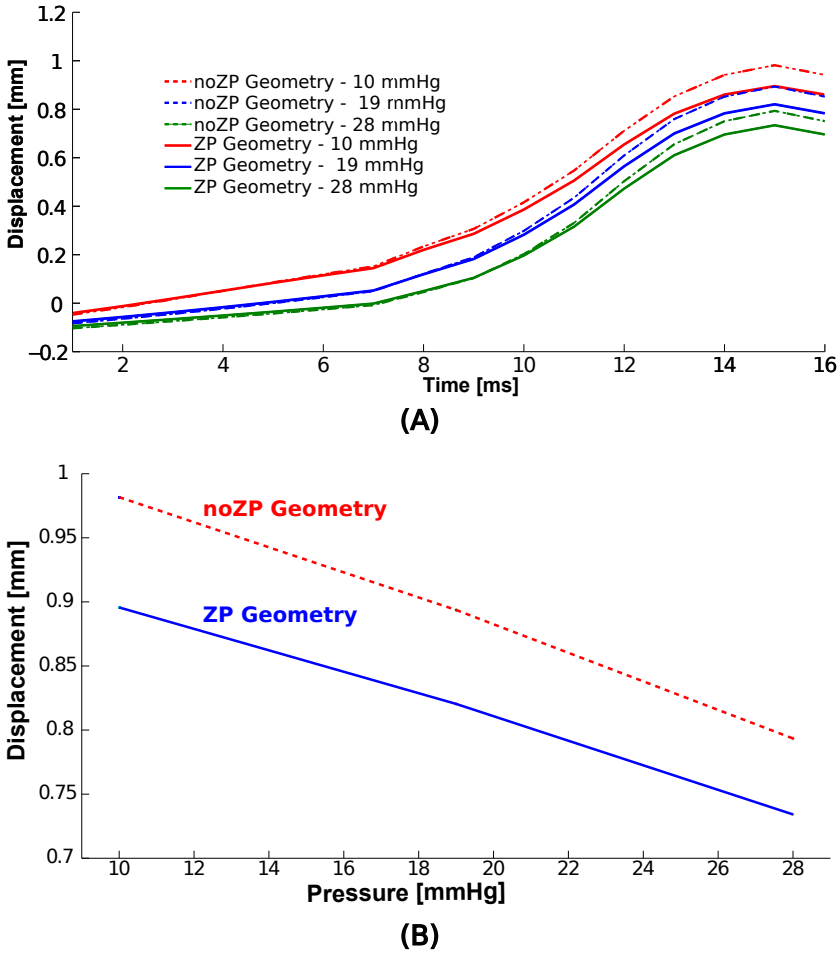

Fig. 7 Effect of the initial stress in the healthy eye. (A) Evolution of the apical displacements for different IOP: i) zero pressure model (discontinuous lines), and ii) image based model (continuous line). (B) Maximum apical displacement for different IOP.

Table 4 shows the percentage increase in the apical displacement due to the initial corneal stress for different IOP and all three geometries. The table shows that the KTC experiences the largest increment in apical displacement, whereas the lowest increment in displacement is obtained for the healthy eye. This correlates well with the lower corneal pachymetry associated with the KTC and post-LASIK geometries.[1]

IOP	$\Delta_U^{\text{apical}} = 100 \cdot (U_{noZP}^{\text{apical}} - U_{ZP}^{\text{apical}})/U_{ZP}^{\text{apical}}$ (%)		
(mmHg)	**Healthy**	**KTC**	**LASIK**
10	7.5	17.5	15.5
19	8.2	20	13.8
28	3.1	18.9	16.5

Table 1 Displacement difference between pressurized geometry (no zero pressure geometry originally measured by the topographer) and zero pressure geometry (obtained from the free-stress algorithm) for three different geometries and IOP

To gain a better understanding on the effect of the initial corneal stress, and to demonstrate the potentiality of the proposed methodology, a population of 130 patients: 53 healthy eyes, 63 KTC eyes and 14 post-LASIK eyes was analysed. In order to validate the model, and the methodology, results form the numerical simulation where compared with clinical results obtained in different studies over 60 Healthy and KTC eyes[22], and 52 LASIK eyes 30 days after surgery[9]. In addition to the apical displacement, the minimum principal stress and stretch at the apex of the anterior surface (σ_{min}^{Apx} and λ_{min}^{Apx} respectively) have been considered in this study.

Table 5 shows the mean and standard deviation of the three biomarkers obtained for the three populations with the image based model and the zero pressure model. Clinical results are also shown for completeness.

Image based model			
Biomarker	**Healthy**	**KTC**	**LASIK**
Apex Pac. [μm]	553.8± 36.2	472.1± 69.3	501.1± 53.9
U [mm]	1.042± 0.136	1.204± 0.193	1.151± 0.114
σ_{min}^{Apx} [MPa]	-0.476± 0.075	-0.624± 0.156	-0.556± 0.078
λ_{min}^{Apx} [–]	0.959± 0.002	0.955± 0.003	0.957± 0.002
Zero pressure model			
Biomarker	**Healthy**	**KTC**	**LASIK**
U [mm]	0.928± 0.110	1.065± 0.166	1.033± 0.097
σ_{min}^{Apx} [MPa]	-0.440± 0.071	-0.573 ± 0.138	-0.520± 0.077
λ_{min}^{Apx} [–]	0.960 ± 0.002	0.956± 0.003	0.958± 0.002
Clinical Results			
Biomarker	**Healthy**	**KTC**	**LASIK**
Apex Pac. [μm]	520± 25	475± 38	524.00± 63.21
U [mm]	1.04± 0.10	1.13± 0.12	1.08± 0.14

Table 2 Statistics of numerical results: i) Maximum Apical Displacement (U [mm]), ii) Minimum in-plane principal stresse at the apex of the anterior corneal surface, σ_{min}^{Apx} [MPa], and iii) Minimum in-plane principal stretch at the apex of the anterior corneal surface, λ_{min}^{Apx} [–], computed with the image based and zero pressure models. Clinical results are also included[22,9] (mean ± standard deviation)

Results for the apical displacement in Table 5 are within the range obtained in clinical studies. However, apical displacements obtained with the zero pressure model underestimate the clinical results, whereas results obtained with the image based model overestimate the maximum apical displacement. Hence, accounting for the initial corneal stress, yields a stiffer corneal response. A two sample Kolmogorov-Smirnov test on the apical displacement obtained with the image based and the zero pressure models have shown no significant differences (p–value > 0.05) between LASIK–KTC, but have shown significant differences between Healthy–KTC and Healthy–LASIK in agreement with clinical results.[22,9] Same results were found for the stress and stretch biomarkers. When comparing the results obtained with the zero pressure model and the image based model, significant differences where found for the healthy eye in all three biomarkers. However, for the KTC and LASSIK eye, significant differences were only found for the maximum apical displacement.

Figure 17 shows the percentage difference between the biomarkers computed with the image based model and the zero pressure model during the air-puff (the zero pressure model is taken as reference). The figure shows a larger dispersion in all biomarkers for the KTC cases as compare to the HEALTHY and LASIK populations. The figure also demonstrates the stiffer response of the cornea when the initial corneal stress is considered, as the apical displacement results always smaller for the image based model than for the zero pressure model. Note that this happens at all moments during the air puff, but becomes more relevant as the pressure of the air-puff increases (at 15 ms in the figure), coinciding with the

maximum deformation of the cornea, and when the nonlinear response of the material becomes more significant.

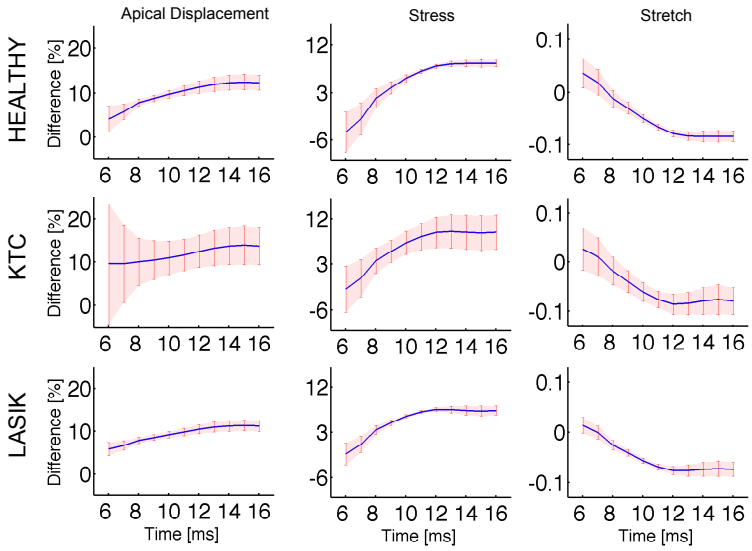

Fig. 8 Percentage difference of the biomarkers between the image based model and the zero pressure model (blue line is the average response and and red bars the dispersion) at each instant during the air-puff. First row corresponds to the Healthy population, second row the KTC population, and third row the LASIK population. Left column corresponds to the apical displacement, U; Middle column to the minimum in-plane principal stress at the apex of the anterior surface of the cornea, σ_{min}^{Apx}; Right column to the minimum in-plane principal stretch at the apex of the anterior surface of the cornea, λ_{min}^{Apx}.

Table 6 summarises the percentage difference in the biomarkers for the high concavity time (t = 15 ms). It is remarkable that the average percentage difference for each biomarker is very similar for the three populations, with a significant larger dispersion in the case of KTC eyes.

Biomarker	**Difference (%)**		
	Healthy	**KTC**	**LASIK**
Maximum concavity time			
U	12.162± 2.217	13.043 ± 5.039	11.339 ± 1.253
σ_{min}^{Apx}	8.358± 0.730	8.873± 3.442	7.194 ± 1.011
λ_{min}^{Apx}	-0.084± 0.012	-0.075± 0.029	-0.072 ± 0.015

Table 3 Biomarkers difference at the beginning of the air-puff and at the high concavity time for the three populations. Results given as mean ± standard deviation.

4 Discussion

A novel automatised methodology for generating a finite element model incorporating patient-specific corneal topographic data amenable for numerical simulation is proposed. Contrary to previous proposed methodologies[23,25], the proposed approach does not approximates the topographical data where it is known, increasing the fidelity of the reconstructed patient model (see Fig. 11C). An implementation of

the proposed pipeline using Matlab and ABAQUS takes about one hour to complete on a single patient: approximately 30 minutes in the model construction phase, and about 30 minutes for the finite element simulation (including the zero pressure algorithm) in a conventional PC with 8 cores and 8 GBRAM. A more optimised implementation of the pipeline could substantially reduce these times, making the proposed methodology feasible for used in clinic as an aided-diagnosis tool. Further, the mesh sensitivity analysis has demonstrated the importance of the finite element mesh used in the computations, in particular when modelling a non-contact tonometry test for which the bending behaviour of the cornea must be captured accurately.[14, 28] In this regard, linear (four nodes tetrahedra) or trilinear elements (eight nodes hexahedra) must be used with care since these elements do not capture the bending behaviour accurately. A sufficiently large number of elements through the thickness must be used in order to achieve accurate results (see Fig. 13B). In this regard, the best compromise between numerical accuracy and computation time, when modelling anon contact tonometry test, was obtained with 20-node quadratic elements and 5 elements through the corneal thickness.

The methodology has been tested on a population of 130 patients (53 healthy eyes, 63 KTC eyes and 14 post-LASIK) by simulating a non-contact tonometry test and comparing numerical results to clinical results obtained with a CorVis ST. However, our simulation was not pretended to model a particular commercial device, but only to replicate a typical evaluation test. Hence, the main characteristics of the test such as the peak pressure of the air-puff, and the location and duration of the air pulse, were set in order to emulate a general non-contact tonometer. In addition, some assumptions were made regarding the air pressure over the cornea. Even though the pressure has been assumed to varied in time and space (see Fig. 13A), shear effects on the corneal surface due to the air-puff has been neglected. In addition, a displacement boundary on the sclera which allows for the radial motion in the sagital Π plane has been used (see Fig. 12C), instead of a zero displacement condition,[23, 25] since it represents a more realistic situation.

Our results indicate that the initial stress of the cornea due to the IOP stiffens the corneal response, leading to significant differences in the apical displacement obtained with the zero pressure model and the image based model. In addition, results for the KTC population show a considerable larger dispersion as compared to the Healthy and the LASIK population. This large variation correlates with the larger dispersion present in the pachymetry data for the KTC eyes. This is in agreement with results from a recent study that show the important effect of the corneal thickness on the corneal response when subjected to a non contact tonometry test.[1] When subjected to an air-puff, the cornea passes from a pure tensile membrane state of stress due to the IOP, to a bending state of stress where the anterior surface experiences contraction while the posterior surface is in traction (see Fig. 18). This explains the significant sensitivity of the results to changes in corneal pachymetry, since the bending stiffness follows an inverse cubic relationship with the corneal thickness. In this line of results, the study conducted on Healthy, KTC

and LASIK gave values for the apical displacements within the range of clinical results[22,26,9,12] even though all models have used the same corneal material and IOP, which leads to think that geometrical features could be more important than corneal tissue considerations when only the apex displacement is studied.

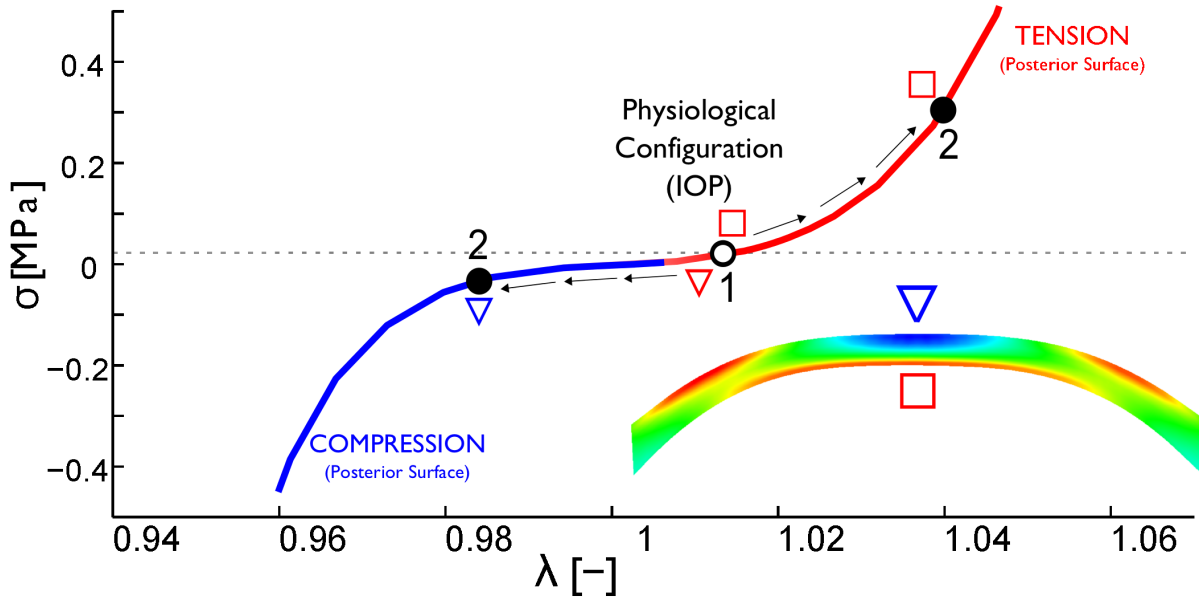

Fig. 9 Apex Stress-Stretch Behaviour for the Healthy Eye with an IOP of 19 mmHg. At the beginning of the simulation (1. Physiological configuration after Zero Pressure Algorithm), both surfaces start at $\lambda > 1$ (physiologic prestress) but, when an air–puff is applied onto the cornea, the cornea bends, the anterior surface (inverted triangle at point 2) works in compression and shortens its length (stretch less than 1 (*blue*)), whereas the posterior surface (square at point 2) works in tension and the local corneal tissue lengthens (stretch greater than 1 (*red*)).

Regarding the proposed pull-back algorithm used to find the free-stress configuration of the eye, even though the algorithm is similar to other approaches proposed in the literature[19,23,7], the present methodology has the advantage of incorporating a consistent mapping of the collagen fibbers into the current zero pressure configuration. Our simulations show that the proposed algorithm found the zero-pressure geometry in less than 5 iterations with a tolerated relative error of less than 1% (MIGUEL ANGEL puedes verificar esto?). Our results also showed that the proposed algorithm preserved the tissue volume globally, i.e. the zero-pressure and image-based geometries had the same volume. This is particularly important for three-dimensional solid simulations, since the corneal and sclera are considered as incompressible. This feature is consequence of using a quasi-incompressible material description for the different tissues. However, this kinematic restriction cannot be guaranteed at element level (Gauss points), as we observed local volume changes greater than XX Tendriamos que hacer un pequeño cálculo de esto. Visto que tienes en el matlab implementado el pull-back, lo puedes verificar para uno de los ejemplos. Yo me espero que en el ojo, a nivel local el volumen se conserve mucho mas. It is important to

point out that the proposed methodology is not absent of numerical problems due to distortion of the mesh during the iterative process, in particular for rather complicated geometries. However, the polar symmetry of the eye model prevents this problem to occur since the initial pre-stress induces only a radial contraction.

The study presents a number of limitations. We have used the same material properties for the cornea and the limbus for all patients, instead of patient specific material parameters. However, the available human data in the literature is limited to pressure-apical rise curves on a limited number of patients. Thus providing only a range of mechanical response. Therefore, we have decided to use a particular set of parameters fitting a particular curve within the reported range as shown in Fig. 12B. Also, the material model could be improved by considering the viscoelastic behaviour.[14] Unfortunately, we did not have access to patient-specific IOP and used instead mean IOP pressures reported in the literature for all our cases. Using patient-specific IOP data would have directly influenced the predicted apical displacement as well as the stress and strain fields, but would not have changed our conclusions regarding the importance of using the zero-pressure geometry, or the potentiality of the proposed modelling pipeline.

In conclusion, a novel in-silico methodology for generating a FE model incorporating patient specific corneal geometry has been proposed. The pipeline allows to perform tests in-silico to carry out a sensitivity analysis of the mechanical properties of the corneal tissue, the influence of the IOP and the geometry of the cornea, on the corneal deformation of patient specific geometric eye models. This allows to improve the understanding of the eye biomechanics, as well as helping to plan surgeries, i.e., LASIK surgeries, or to interpret the results of new diagnosis tools, as in the case of non-contact tonometers.

5 Acknowledgments

The research leading to these results has received funding from the European Union's Seven Framework Program managed by REA Research Executive agency http://ec.europa.eu/research/rea (FP7/2007-2013) under Grant Agreement FP7-SME-2013 606634 and the Spanish Ministry of Economy and Competitiveness (DPI2011-27939-C02-01 and DPI2014-54981R).

References

1. M.A. Ariza, J.F. Zuria, D.P. Piñero, J.F. Rodriguez-Matas, B. Calvo. Coupled Biomechanical Response of the Cornea Assessed by Non-Contact Tonometry. A simulation study. *PLOS One*, 2015 (in press).
2. V. Alastrué, B. Calvo, E. Peña, and M. Doblaré. Biomechanical modelling of refractive corneal surgery. *J Biomech Eng*, 128(1):150–160, Feb 2006.
3. Jean-Louis Bourges, Nicolas Alfonsi, Jean-François Laliberté, Miguel Chagnon, Gilles Renard, Jean-Marc Legeais, and Isabelle Brunette. Average 3-dimensional models for the comparison of orbscan ii and pentacam pachymetry maps in normal corneas. *Ophthalmology*, 116(11):2064–2071, Nov 2009.
4. Bryant, M.R., P.J. McDonnell. Constitutive laws for biomechanical modelling of refractive surgery. *J. Biomech. Eng*, 118(4): 473–481, 1996.
5. George C. Runger Douglas C. Montgomery. *Applied statistics and probability for engineers*, volume 1. New York: John Wiley & Sons, 2nd edition, 1999. ISBN : 9780471170273.
6. Armin Eilaghi, John G. Flanagan, Inka Tertinegg, Craig A. Simmons, G. Wayne Brodland, and C. Ross Ethier. Biaxial mechanical testing of human sclera. *J Biomech*, 43(9):1696–1701, Jun 2010.
7. Ahmed Elsheikh, Charles Whitford, Rosti Hamarashid, Wael Kassem, Akram Joda, and Philippe Büchler. Stress free configuration of the human eye. *Med Eng Phys*, 35(2):211–216, Feb 2013.
8. T Christian Gasser, Ray W. Ogden, and Gerhard A. Holzapfel. Hyperelastic modelling of arterial layers with distributed collagen fibre orientations. *J R Soc Interface*, 3(6):15–35, Feb 2006.
9. Ziad Hassan, Laszlo Modis, Jr, Eszter Szalai, Andras Berta, and Gabor Nemeth. Examination of ocular biomechanics with a new scheimpflug technology after corneal refractive surgery. *Cont Lens Anterior Eye*, May 2014.
10. Gerhard A Holzapfel, Thomas C Gasser, and Ray W Ogden. A new constitutive framework for arterial wall mechanics and a comparative study of material models. *Journal of elasticity and the physical science of solids*, 61(1-3):1–48, 2000.
11. Jiaxu Hong, Jianjiang Xu, Anji Wei, Sophie X. Deng, Xinhan Cui, Xiaobo Yu, and Xinghuai Sun. A new tonometer–the corvis st tonometer: clinical comparison with noncontact and goldmann applanation tonometers. *Invest Ophthalmol Vis Sci*, 54(1):659–665, Jan 2013.
12. Tukezban Huseynova, George O Waring, 4th, Cynthia Roberts, Ronald R. Krueger, and Minoru Tomita. Corneal biomechanics as a function of intraocular pressure and pachymetry by dynamic infrared signal and scheimpflug imaging analysis in normal eyes. *Am J Ophthalmol*, 157(4):885–893, Apr 2014.
13. Sabine Kling and Susana Marcos. Contributing factors to corneal deformation in air puff measurements. *Invest Ophthalmol Vis Sci*, 54(7):5078–5085, Jul 2013.
14. Sabine Kling, Nandor Bekesi, Carlos Dorronsoro, Daniel Pascual, and Susana Marcos. Corneal viscoelastic properties from finite-element analysis of in vivo air-puff deformation. *PLoS One*, 9(8):e104904, 2014.
15. Elena Lanchares, Begoña Calvo, José A. Cristóbal, and Manuel Doblaré. Finite element simulation of arcuates for astigmatism correction. *J Biomech*, 41(4):797–805, 2008.
16. R. H. Newton and K. M. Meek. The integration of the corneal and limbal fibrils in the human eye. *Biophys J*, 75(5): 2508–2512, Nov 1998.
17. Kelechi C. Ogbuehi and Uchechukwu L. Osuagwu. Corneal biomechanical properties: precision and influence on tonometry. *Cont Lens Anterior Eye*, 37(3):124–131, Jun 2014.
18. A. Pandolfi and F. Manganiello. A model for the human cornea: constitutive formulation and numerical analysis. *Biomech Model Mechanobiol*, 5(4):237–246, Nov 2006.
19. Anna Pandolfi and Gerhard A. Holzapfel. Three-dimensional modelling and computational analysis of the human cornea considering distributed collagen fibril orientations. *J Biomech Eng*, 130(6):061006, Dec 2008.

20. Peter M. Pinsky, Dolf van der Heide, and Dimitri Chernyak. Computational modelling of mechanical anisotropy in the cornea and sclera. *J Cataract Refract Surg*, 31(1):136–145, Jan 2005.
21. Fabián Riveros, Santanu Chandra, Ender A. Finol, T Christian Gasser, and Jose F. Rodriguez. A pull-back algorithm to determine the unloaded vascular geometry in anisotropic hyperelastic aaa passive mechanics. *Ann Biomed Eng*, 41 (4):694–708, Apr 2013.
22. Cynthia Roberts. A journey through the biomechanics of the cornea. In *Conference ESOIRS*, Ohio, USA, May 2012. The Ohio State University.
23. Abhijit Sinha Roy and William J Dupps, Jr. Patient-specific modelling of corneal refractive surgery outcomes and inverse estimation of elastic property changes. *J Biomech Eng*, 133(1):011002, Jan 2011.
24. Pablo R. Ruiseñor Vázquez, Jonatán David Galletti, Natalia Minguez, Marianella Delrivo, Fernando Fuentes Bonthoux, Tomás Pförtner, and Jeremías Gastón Galletti. Pentacam scheimpflug tomography findings in topographically normal patients and subclinical keratoconus cases. *Am J Ophthalmol*, 158(1):32–40.e2, Jul 2014.
25. Harald P. Studer, Hansjörg Riedwyl, Christoph A. Amstutz, James V M. Hanson, and Philippe Büchler. Patient-specific finite-element simulation of the human cornea: a clinical validation study on cataract surgery. *J Biomech*, 46 (4):751–758, Feb 2013.
26. Bruno Freitas Valbon, Renato Ambrósio, Jr, Bruno Machado Fontes, and Milton Ruiz Alves. Effects of age on corneal deformation by non-contact tonometry integrated with an ultra-high-speed (uhs) scheimpflug camera. *Arq Bras Oftalmol*, 76(4):229–232, 2013.
27. Joe F. Thompson; Bharat K. Soni; Higel P. Weatherill. *Handbook of Grid Generation*. CRC Press, 1998. ISBN: 978-0849326875.
28. Charles Whitford, Harald Studer, Craig Boote, Keith M. Meek, and Ahmed Elsheikh. Biomechanical model of the human cornea: Considering shear stiffness and regional variation of collagen anisotropy and density. *Journal of the Mechanical Behavior of Biomedical Materials*, (0):–, 2014. ISSN 1751-6161.